Available online at www.sciencedirect.com
ScienceDirect
Aerosol Science 37 (2006) 1840–1852
Journal of Aerosol Science
www.elsevier.com/locate/jaerosci

The experimental transfer function of the Couette centrifugal particle mass analyzer

J.S. Olfert[a,*], K.StJ. Reavell[b], M.G. Rushton[b], N. Collings[a]

[a] *Hopkinson Laboratory, Engineering Department, Cambridge University, Trumpington Street, Cambridge, CB2 1PZ, UK*
[b] *Cambustion Ltd., J6 The Paddocks, 347 Cherry Hinton Road, Cambridge, CB1 8DH, UK*

Received 2 March 2006; received in revised form 29 July 2006; accepted 31 July 2006

Abstract

The Couette centrifugal particle mass analyzer (CPMA) classifies particles by their mass-to-charge ratio. Unlike the aerosol particle mass (APM) analyzer, the Couette CPMA uses a stable system of forces to improve the transfer function of the classifier. A prototype Couette CPMA has been built and tested. The experimental results from the prototype agree well with theory and it is found that indeed the transfer function of the Couette CPMA is better than the APM's. Experimental work is shown using a differential mobility analyzer (DMA) and Couette CPMA to classify polystyrene latex (PSL) and di-2-ethylhexyl sebacate (DEHS) particles. By measuring the mass of PSL particles the absolute uncertainty of the Couette CPMA was found to be 6.7–38% higher in terms of mass (or 2.2–11% higher in terms of equivalent diameter) than the expected value. However, when the DMA–CPMA system was calibrated with PSL particles the density of DEHS particles was measured to within approximately 3% of the expected value.

Keywords: Particle mass; Particle density; Centrifugal particle mass analyzer

1. Introduction

The Couette centrifugal particle mass analyzer (CPMA) is an instrument that classifies particles by their mass. Mass measurements from the Couette CPMA can be combined with other data to determine important particle properties. For example, particle properties such as effective density, fractal dimension, and dynamic shape factor can be found if particle mass and mobility diameter are measured with a Couette CPMA and differential mobility analyzer (DMA), respectively. The Couette CPMA consists of two rotating coaxial cylindrical electrodes rotating at different angular velocities (see Fig. 1). Pre-charged particles pass between the electrodes where they experience electrostatic and centrifugal forces (F_e and F_c, respectively) acting in opposite directions. Particles also experience a drag force which opposes the direction of motion. Particles of a particular mass-to-charge ratio will pass through the Couette CPMA, depending on the rotational speed and voltage difference between the electrodes. If the charge on the particles is known then the mass of the classified particles is known. The trajectory of particles in the radial (r) direction is

* Corresponding author. Tel.: +44 1223 332681; fax +44 1223 339906.
E-mail address: j.s.olfert.03@cantab.net (J.S. Olfert).

0021-8502/$ - see front matter © 2006 Elsevier Ltd. All rights reserved.
doi:10.1016/j.jaerosci.2006.07.007

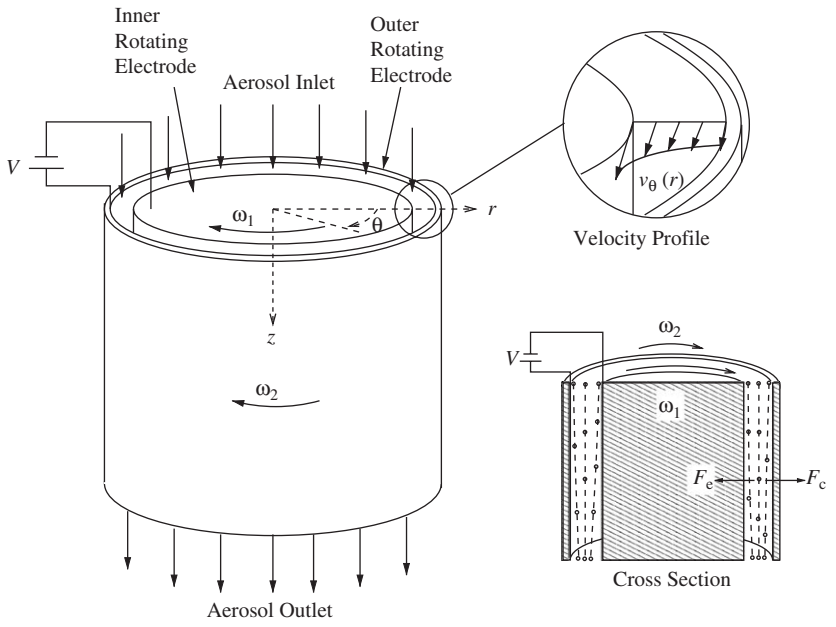

Fig. 1. Schematic of the Couette centrifugal particle mass analyzer.

given by (Olfert & Collings, 2005):

$$\frac{m}{\tau}\frac{\mathrm{d}r}{\mathrm{d}t} = \frac{m v_\theta(r)^2}{r} - \frac{neV}{r\ln(r_2/r_1)}, \tag{1}$$

where m is the mass of the particle, τ is the particle relaxation time, t is the time, $v_\theta(r)$ is the velocity profile of the aerosol flow in the angular direction, n is the number of elementary charges on the particle, e is the unit electrical charge (1.6×10^{-19} C), r_1 and r_2 are the inner and outer radii of the electrodes, and V is the voltage difference between the two electrodes.

The Couette CPMA design represents a significant improvement over the aerosol particle mass (APM) analyzer. The APM, developed by Ehara et al. (Ehara, 1995; Ehara, Hagwood, & Coakley, 1996), operates in a similar manner to that of the Couette CPMA; however, unlike the Couette CPMA, the APM's inner and outer electrodes rotate at the same angular velocity. In the APM there is an unstable system of external forces acting on the particles. The external forces in the APM are the centrifugal force which is proportional to r and the electrostatic force which is proportional to $1/r$ (where r is the distance from the center of rotation). A particle of the correct mass-to-charge ratio will be balanced at the 'equilibrium radius', r^*. If the particle is positioned so that $r > r^*$ the centrifugal force will be greater than the electrostatic force and the particle will move towards the outer electrode. Depending on the force imbalance, the axial flow velocity, length of classifier, and drag on the particle, the particle may impact on the outer electrode. Similarly, particles may impact on the inner electrode if they are positioned at $r < r^*$. The unstable system of forces cause the transfer function of the APM to be greatly reduced in certain operating conditions.

Reavell and Rushton (2004) suggested two new CPMA[1] concepts to create a stable system of external forces acting on the particle in the radial direction. Firstly, in the Fluted CPMA the geometry of the electrodes can be changed using reversed 'scooped' sections so that the magnitude of the electrostatic force increases with radius rather than decrease (Olfert, 2005). However, in the Fluted CPMA the forces will be unstable in the angular direction which again reduces the transfer function although the performance of the Fluted CPMA is still better than the APM. Secondly, in the Couette CPMA the inner electrode rotates slightly faster than the outer electrode (Olfert & Collings, 2005). This creates a concave velocity profile between the electrodes (known as Couette flow; see Fig. 1) such that the centrifugal

[1] In this paper the term 'CPMA' will refer to instruments that use a centrifugal and electrostatic force to classify particles by their mass-to-charge ratio; i.e. the APM, Couette CPMA, and Fluted CPMA.

force on the particle will decrease as the radius increases. With this system, particles of the correct mass-to-charge ratio move toward the equilibrium radius and the transfer function is greatly improved compared to the APM. It was shown in an earlier paper (Olfert, 2005) that, theoretically, the Couette CPMA offers the best performance of all three classifiers.

The shape of the transfer function of the classifiers is determined by one dimensionless constant, λ (Ehara et al., 1996; Olfert, 2005; Olfert & Collings, 2005). For the Couette CPMA, λ is defined as

$$\lambda = \frac{L/\bar{v}_z}{1/\{2\tau[(\omega_1(\hat{r}^2-\hat{\omega})/(\hat{r}^2-1))^2 - (\omega_1 r_1^2(\hat{\omega}-1)/(\hat{r}^2-1))^2/r^{*4}]\}} = \frac{L/\bar{v}_z}{1/[2\tau(\hat{\alpha}^2-\hat{\beta}^2/r^{*4})]}, \tag{2}$$

where L is the length of the classifier, $\bar{v}_z$ is the average flow velocity in the axial direction, τ is the particle relaxation time, ω_1 and ω_2 are the inner and outer electrode angular velocities, $\hat{\omega} = \omega_2/\omega_1$, $\hat{r} = r_1/r_2$, and r^* is the equilibrium radius. For the APM and Fluted CPMA, λ is similar to Eq. (2) except that $\omega_1 = \omega_2 = \omega$ resulting in

$$\lambda = \frac{L/\bar{v}_z}{1/2\tau\omega^2}. \tag{3}$$

As $|\lambda|$ increases, the width of the transfer function will decrease (Olfert, 2005). A relatively long classifier, slow flow rate, large angular velocity, or large particle will result in a large value of $|\lambda|$ and a narrower transfer function.

A prototype of the Couette CPMA has been built. In this paper, experimental results from this prototype Couette CPMA are compared to the theoretical models described by Olfert and Collings (2005). The Couette CPMA is also compared experimentally to the APM. Finally, a DMA and Couette CPMA system is used to measure the density of di-2-ethylhexyl sebacate (DEHS) particles to show the uncertainty of the DMA–CPMA system when it is calibrated with polystyrene latex (PSL) particles.

2. Prototype design

A schematic of the prototype Couette CPMA is shown in Fig. 2. The aerosol enters the instrument through the hollow shaft (on the left-hand side of the figure) and travels through the shaft until it enters the region between the two electrodes by passing through cross-drilled holes in the shaft. The particles then move radially toward the classification region. Before the classification region the particles pass through a bend where some particles may impact onto the wall. The particles that enter the classification region will move with a trajectory described previously (Olfert & Collings, 2005), where particles of the correct mass-to-charge ratio will reach the end of the classification region. Particles of an incorrect mass-to-charge ratio will impact onto the electrodes and are assumed to stick. The particles that are classified then turn another bend and move radially toward the shaft where they again pass through cross-drilled holes into the center of the shaft and exit the instrument. In the prototype, $r_1 = 25$, $r_2 = 26.5$, and $L = 50$ mm.

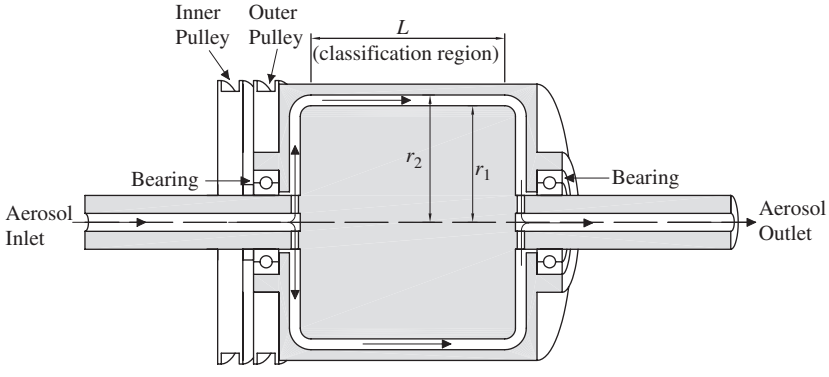

Fig. 2. Schematic of the prototype Couette CPMA.

The electrodes of the Couette CPMA are driven by one brushless DC motor. On the motor's shaft are mounted two toothed pulleys that drive toothed pulleys attached to the inner and outer electrodes. The pulleys on the electrodes and the pulley on the motor shaft that drives the inner electrode all have 60 teeth. The speed ratio between the inner and outer electrodes can be changed by simply changing the toothed pulley on the motor shaft which drives the outer electrode. For this prototype we have used sizes of 60, 56, 54, and 52 teeth. Therefore, speed ratios ($\hat{\omega}$) of 1, 0.933, 0.900, and 0.867 were used. When the speed ratio is unity the Couette CPMA will operate as if it is an APM.

3. Experimental setup and procedure

A schematic of the experimental setup is shown in Fig. 3. The types of particles used in this experiment were PSL (Duke Scientific 3000 series) and DEHS. The DEHS particles and the PSL particles $\geqslant 102$ nm were generated with a Collison atomizer. The PSL particles were generated in a solution of deionized water while the DEHS particles were generated in a solution of 2-propanol (HPLC grade) with a concentration of 0.1% volume of DEHS. The particles were passed through a silica gel diffusion dryer, if the particles were generated in a water solution (i.e. PSL), or through activated carbon, if they were generated in a hydrocarbon solution (i.e. DEHS). PSL particles are packaged in an aqueous solution containing surfactant. When the PSL particles are atomized with a Collison atomizer a distribution of surfactant particles are also generated. The surfactant particles are formed when atomized droplets, that do not contain any PSL spherules, are evaporated to a surfactant core when they pass through the diffusion dryer. The surfactant particles are generally less than 100 nm in size, but the distribution will depend on the atomizer and concentration of PSL solution. Therefore, the 50 and 73 nm PSL particles were generated with a TSI electrospray aerosol generator (TSI model number 3480), which has a smaller initial droplet size ($\sim$ 150 nm). Since the electrospray produces smaller initial droplets, the remaining surfactant particle cores after evaporation will be much smaller than particles generated with a Collison atomizer. Therefore, the surfactant particles can be distinguished from the PSL particles.

All of the generated particles were passed through a charge neutralizer where they obtained a Boltzmann equilibrium charge distribution. Particles were classified by mobility diameter with the DMA (TSI model number 3080); when PSL particles were classified, the DMA voltage was adjusted to give a maximum penetration of particles, thereby calibrating the DMA for that size of particle. Condensation particle counters (CPCs) were used to measure the particle concentration before and after the Couette CPMA (CPC_1, TSI model number 3022A; CPC_2, TSI model number 3025A). The aerosol not counted by CPC_1 enters the Couette CPMA where it is classified by mass. The particles exiting the Couette CPMA are counted with CPC_2.

The Couette CPMA was set at a constant rotational speed for each test and the voltage was stepped. The transfer function of the Couette CPMA was recorded for each voltage step where the experimental transfer function (Ω_{exp}) is

$$\Omega_{exp} = \frac{N_{CPC_2}}{N_{CPC_1}}, \tag{4}$$

where N_{CPC_1} and N_{CPC_2} are the number concentrations from CPC_1 and CPC_2, respectively.

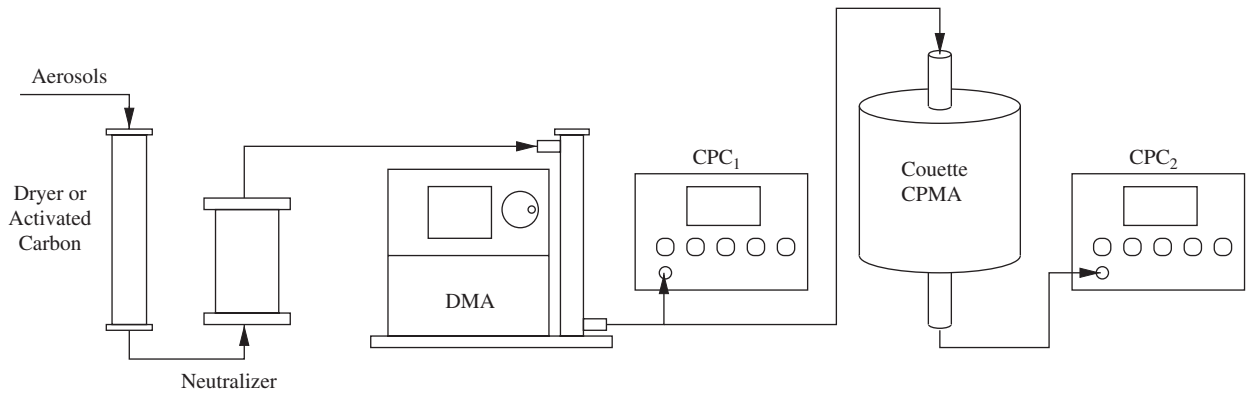

Fig. 3. Schematic of the experimental setup.

For a monodisperse aerosol (like that exiting the DMA) the transfer function of the Couette CPMA will be maximum when the centrifugal and electrostatic forces are balanced at the center of the gap between the electrodes (i.e. $r^* = r_c$). At this point the drag force will be zero and the mass of particles exiting the Couette CPMA will be (see Eq. (1))

$$m = \frac{neV_c}{\omega_c^2 r_c^2 \ln(r_2/r_1)}, \tag{5}$$

where V_c is the voltage at which the transfer function is maximum and ω_c is the angular velocity at r_c (i.e. $\omega_c = v_\theta(r_c)/r_c$).

To find V_c for the discrete data set, the data must be fitted so that the maximum of the transfer function can be found. The experimental data was fitted using the method of least squares, where the χ_f^2 function is minimized, where

$$\chi_f^2 = \sum_{i=1}^{m} \left(\frac{\Omega_{\text{exp},i} - \Omega_{\text{model},i}}{\sigma_i} \right)^2, \tag{6}$$

where σ_i is the error estimate of data point i and $\Omega_{\text{exp},i}$ and $\Omega_{\text{model},i}$ are the experimental and model transfer functions of data point i, respectively. In this study, σ_i^2 was set to equal $1/\Omega_{\text{model},i}$. This places greater value on the points near the maximum of the transfer function. This was done to minimize the effect of skewed distributions, which are discussed in Section 4.1. The $\Omega_{\text{model},i}$ is found from a computational model describing the transfer function. For the PSL particles, either the diffusion or non-diffusion theoretical models described previously (Olfert & Collings, 2005),[2] were used depending on whether diffusion was significant for the particle being classified. These models assume that the particles entering the Couette CPMA are strictly monodisperse (i.e. all of the exact same particle size), which is an adequate approximation for the narrow distribution of PSL particles. The DEHS particles, which are classified by the DMA, are not strictly monodisperse, and it was found that a normal probability distribution function fit the data better than the previous models. A convolution of the DMA's and Couette CPMA's transfer functions could be used but would be computationally expensive.

The Matlab function `fminsearch` was used to minimize the χ_f^2 function (to a tolerance of 0.1%) by changing the particle density in the model (this shifts the fit curve left–right) and by scaling the amplitude. From the data fit the voltage at the maximum value of the transfer function (V_c) is determined and the mass of the particles corresponding to that voltage can be calculated using Eq. (5).

4. Comparing prototype performance to theory

The performance of the prototype CPMA was tested by comparing experimental results to the theoretical models presented previously (Olfert & Collings, 2005). To do this, PSL particles were classified with the DMA and the Couette CPMA as described in Section 3. PSL particles were chosen as a test particle because they are well known in size, density, and shape. The Couette CPMA was tested by: (1) classifying various sizes of PSL particles, (2) classifying the same size PSL particles with different speed ratios (i.e. varying $\hat{\omega}$), and (3) classifying the same size PSL particles at different operating conditions (i.e. varying λ). Also, a DMA–CPMA system was used to measure the density of DEHS particles to determine the accuracy of such a system when it has been calibrated with PSL particles.

4.1. Classifying various sizes of PSL particles

The Couette CPMA was tested by classifying PSL particles with sizes from 50 to 596 nm. The experimental and theoretical transfer functions of the Couette CPMA for each of the sizes is shown in Fig. 4. The 73–596 nm PSL particle experimental results were fitted to the non-diffusion model and the 50 nm PSL particle data were fitted with the diffusion model. The operating conditions and a summary of the results are shown in Table 1. The figures show the uncertainty in the number measurement by the CPCs (±10%) and the uncertainty in the theoretical model due to the manufacturer's tolerance in the size of the PSL particles (see Table 1). (The uncertainty in the rotational speed and voltage of the Couette CPMA are negligible compared to the uncertainty in the size of the particle.) The results shown

[2] The models in the cited paper used a Taylor series expansion about the point r^* to simplify the analysis. This simplification is only valid if the values of r^* contributing to the transfer function are close to r_c. The models used in this work did not use the Taylor series expansion because it would not be valid under certain conditions shown here.

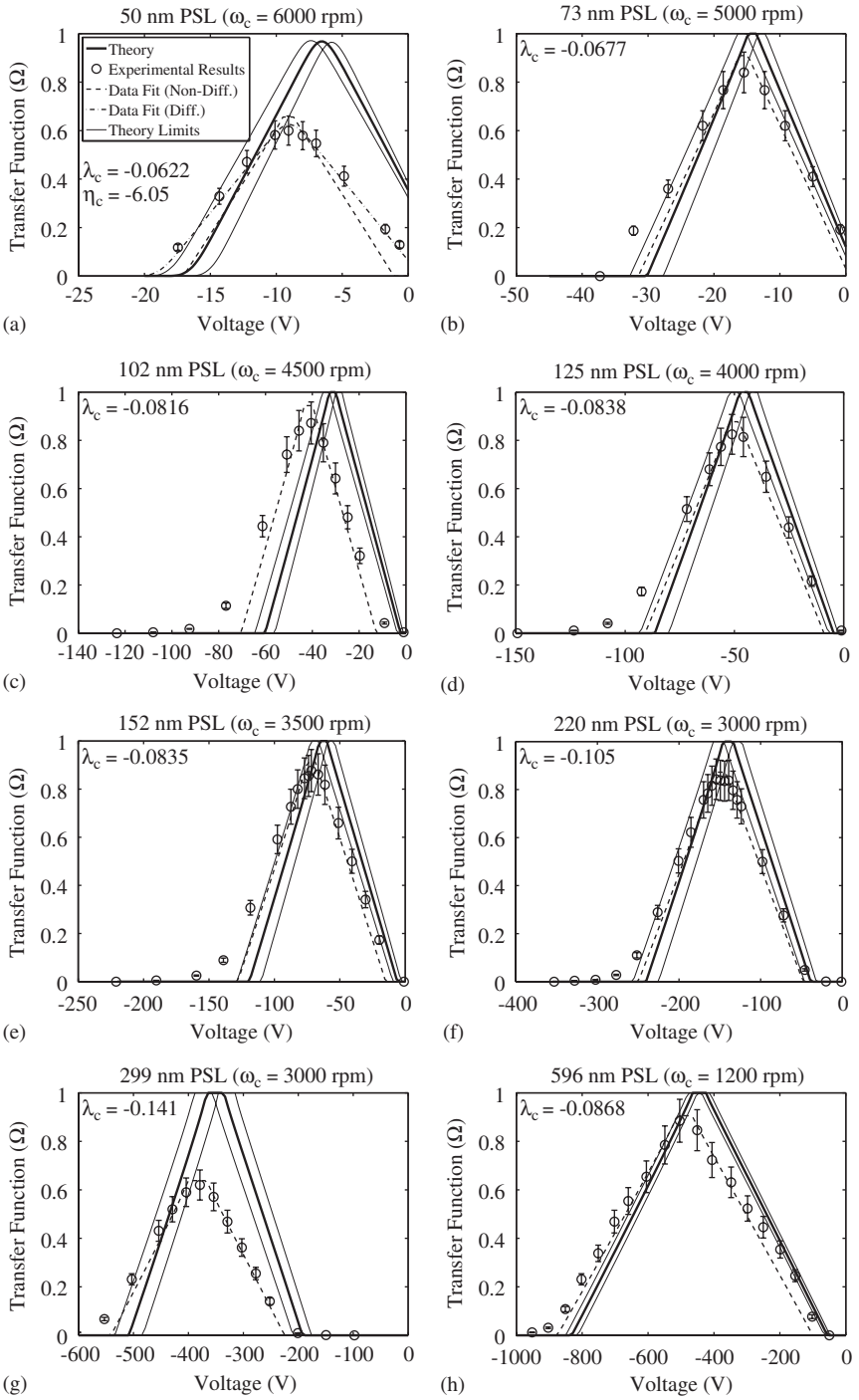

Fig. 4. Theoretical and experimental comparison of Couette CPMA classification of PSL particles.

in the table show that the Couette CPMA consistently over-predicts the mass of the PSL particles. For the PSL particles measured here, the over-estimation in mass ranged from 6.7% to 37.6%, which corresponds to an over-estimation in the equivalent diameter of 3.0–11.2%. It is believed that this systematic error could be caused by two factors: (1) uncertainty in the aerosol velocity profile between the cylindrical electrodes, and/or (2) surfactant or impurities in the atomized PSL/water solution may have increased the mass of the particles.

Table 1
Operating conditions and summary of PSL experiments

PSL dimensions		CPMA settings				Measured dimensions	
d_{PSL} (nm)	m_{PSL} (fg)	ω_c (rpm)	Q_{CPMA} (lpm)	λ_c	V_c (V)	m (% error) (fg)	d_{ma} (% error) (nm)
50 ± 2.0	0.0687	6000	0.3	−0.0622	−9.02	0.0946 (37.6%)	55.6 (11.2%)
73 ± 2.6	0.214	5000	0.3	−0.0677	−15.5	0.234 (9.41%)	75.2 (3.04%)
102 ± 3	0.583	4500	0.3	−0.0816	−40.0	0.746 (27.9%)	111 (8.54%)
125 ± 4	1.07	4000	0.3	−0.0838	−49.9	1.18 (9.77%)	129 (3.16%)
152 ± 5	1.93	3500	0.3	−0.0835	−71.5	2.20 (14.2%)	159 (4.52%)
220 ± 6	5.85	3000	0.3	−0.105	−149	6.25 (6.72%)	225 (2.19%)
299 ± 6	14.7	3000	0.3	−0.141	−383	16.1 (9.36%)	308 (3.03%)
596 ± 6	116	1200	0.3	−0.0868	−488	128 (9.87%)	615 (3.19%)

Firstly, because the fluid dynamics in the Couette CPMA is complex there is uncertainty in the aerosol velocity profile between the two electrodes. In the theoretical model the center rotational speed (ω_c) is found from the Navier–Stokes equation assuming that the electrodes are infinitely long (i.e. end effects are negligible), where the solution is found to be (Taylor, 1923)

$$\omega_c = \hat{\alpha} + \frac{\hat{\beta}}{r_c^2}. \tag{7}$$

(See Eq. (2) for the definition of $\hat{\alpha}$ and $\hat{\beta}$.) In reality the velocity profile of the aerosol in the classification region may be different than the equation above due to entry effects or other complex flows. If the actual ω_c is faster than the expected ω_c, then the measured mass of particles will be heavier than expected. This systemic error can be accounted for by using a calibration standard (such as PSL) as will be shown in Section 4.4.

Secondly, artifacts attached to the PSL particles may have led to higher than expected measurements of mass. It is well known that nebulized PSL may have an outer residue layer of surfactant or it may have a nodule of surfactant or a water impurity attached (Dalley, Greenaway, Ulanowski, Hesse, & Kaye, 2005; Knollenberg, 1989; Zelenyuk, Cai, Chieffo, & Imre, 2005). Megaw and Wells (1972) found that for small PSL particles (less than 100 nm) an added surfactant layer can greatly increase the effective size of the particles. For example, a PSL sphere with a nominal diameter of 50 nm was measured by Megaw and Wells (1972) to have an effective diameter of 58 nm (a difference of 16%). Also, Kasper and Berner (1980), using a cylindrical aerosol centrifuge, found that the difference between nominal and measured PSL particles (with sizes ranging from 176 nm to 2 μm) varied unsystematically by up to 10%. In this study, mass equivalent diameters measured with the Couette CPMA were 2.2–11.2% higher than the manufacturer's stated particle size. Added surfactant may explain the large difference between the nominal and measured diameter of the 50 nm PSL particles measured in this study (11.2%); however, the systematic offset at higher particle sizes is most likely due to the uncertainty in the velocity profile. It should also be noted that a similar experiment was performed by Ehara et al. (1996) classifying 309 nm PSL particles with an APM. In that test, Ehara et al. (1996) under-estimated the mass of particle by 6.5% (or 2.3% in terms of diameter). The absolute uncertainty in the measurement made with the APM is similar in magnitude to the absolute uncertainties measured here for most particle masses.

From Fig. 4 it is also apparent that the amplitude of the transfer function is lower than the model prediction. The theoretical model only predicts the transfer function of the classification region (see Fig. 2). However, many particles may intercept the walls of the classifier before and after the classification region due to inertial effects such as impaction and centrifugal separation. In particular, the right-angled turns directly before and after the classification region will be a major source of particle loss. Particles in that region will have a large centrifugal force and no balancing electrostatic force so particles will be forced toward the outer electrode. Particles may also be lost to the inner shaft as they move down the shaft and through the holes into the space between the electrodes. The role that inertial effects play in reducing the transfer function is seen in Figs. 4f and g where 220 and 299 nm particles are classified at the same rotational speed. It is apparent that the transfer function is reduced due to inertial effects as more of the heavier particles are lost during classification.

The figures in Fig. 4 also show that the transfer functions have a 'tail' on the left side of the figures (i.e. at higher voltages), especially in Figs. 4b–g. The tail may be caused by particles that have had mass added from surfactant or

impurities in the water. Also, the tail could also be caused by singly charged doublets (a doublet is two PSL spheres stuck together), since a doublet particle would be seen at a voltage twice that of V_c.

Fig. 4a shows the experimental data for the classification of 50 nm PSL particles. The theoretical curve shown in the figure is from the diffusion model and the experimental data was fitted to both the diffusion and non-diffusion models. It was shown previously that diffusion effects become important when $|\eta_c|$ is approximately less than 10 (Olfert & Collings, 2005), where η_c is a dimensionless constant that characterizes the effect of diffusion on the classifier. For the PSL measurements shown, $|\eta_c|$ was only less than 10 for the 50 nm PSL test ($\eta_c = -6.05$). Particle diffusion has the effect of broadening and decreasing the amplitude of the transfer function. The figure shows that the diffusion model fits the experimental data very well, while the non-diffusion model is too narrow.

The range of the Couette CPMA is limited by the maximum electrostatic and centrifugal force obtainable. For the prototype, the maximum voltage and rotational speed was 1000 V and 6000 rpm (ω_c), respectively. As seen from Eq. (5), the same particle mass can be classified with infinite combinations of voltage and rotational speed, with narrower transfer functions (to a limit, see Olfert & Collings, 2005) at higher voltages and speeds. To classify a small particle with an adequate transfer function, the rotational speed must be very high. The maximum rotational speed of the prototype Couette CPMA was limited by the PTFE seals used to seal the aerosol from the ambient air. To avoid over-heating the seals, the operational speed was limited to 6000 rpm. For this prototype the smallest particle to be adequately classified was approximately 50 nm. However, PSL particles as small as 10 nm have been classified with an APM using larger diameter electrodes and higher rotational speeds (Fukushima, Tajima, Ehara, & Coakley, 2005). Theoretically, the Couette CPMA could be optimized to operate at higher speeds and measure smaller particles. To measure large particles a low rotational speed and high voltage is required. The prototype was designed to safely operate at a maximum voltage of 1000 V. The maximum voltage obtainable in the Couette CPMA is limited by the dielectric strength of air, the distance between the electrodes, and the voltage rating of the wiring. The Couette CPMA could be operated at a higher voltage by increasing the gap between the electrodes and redesigned wiring.

4.2. Examples concerning differences in $\hat{\omega}$

As mentioned in the Introduction, the performance of CPMAs is highly dependent on the stability of the system of external forces acting on the particles. In the APM the system of external forces are unstable and the amplitude of the transfer function can be much lower than the Couette CPMA. In the Couette CPMA the stability of the system of forces can be changed by changing the speed ratio between the electrodes ($\hat{\omega}$). The stability of the forces can be seen in the dimensionless number, λ. When λ is less than zero the external forces are stable and particles of the correct mass-to-charge ratio will move towards the equilibrium radius; when λ is greater than zero the external forces are unstable. When $\lambda = 0$ the forces are neutrally stable and it can be shown that this will occur when $\hat{\omega} \approx \hat{r}$ (see Eq. (2)), where for the prototype $\hat{r} = r_1/r_2 \approx 0.943$. Therefore, the external forces in the prototype will be stable when $\hat{\omega} \lessapprox 0.943$.

Another consideration relating to the speed ratio is the fluid instability known as Taylor vortices. Taylor vortices are 'a laminar three-dimensional flow pattern consisting of rows of nearly square alternating toroidal vortices' (White, 1994). According to inviscid theory Taylor vortices will develop when $\hat{\omega} < \hat{r}^2$ (Taylor, 1923; although viscous theory allows for a slightly larger difference in rotational speeds). Therefore, to avoid Taylor vortices the speed ratio of the prototype should be greater than $\hat{r}^2$, where for the prototype $\hat{r}^2 = (r_1/r_2)^2 \approx 0.890$.

Figs. 5 and 6 show the transfer functions, both experimental and theoretical, of the Couette CPMA classifying 220 nm PSL particles at the same center rotational speed ($\omega_c = 6000$ rpm) but at four different speed ratios: 1, 0.933, 0.900, and 0.867. For each of the speed ratios the corresponding λ_c are 0.52, −0.098, −0.42, and −0.75, respectively. Note, that when $\hat{\omega} = 1$ (APM mode) the external forces are unstable and when $\hat{\omega} = 0.867$ the fluid is unstable and Taylor vortices will be present. Fig. 5 shows that the transfer function of the Couette CPMA at $\hat{\omega} = 0.933$ and 0.900 are very similar. As before many particles are lost due to inertial effects (about 50% in this case). At this operating condition, theory predicts that the transfer function of the APM should be about 60% of the transfer function of the Couette CPMA and the experimental results agree with that prediction. These results show that the Couette CPMA does have an improved transfer function over that of the APM, but particle losses due to inertial effects in this prototype produce a significant amount of particle loss. Therefore, an improved design is desirable in the region where the particles are introduced to and leave the classifying section.

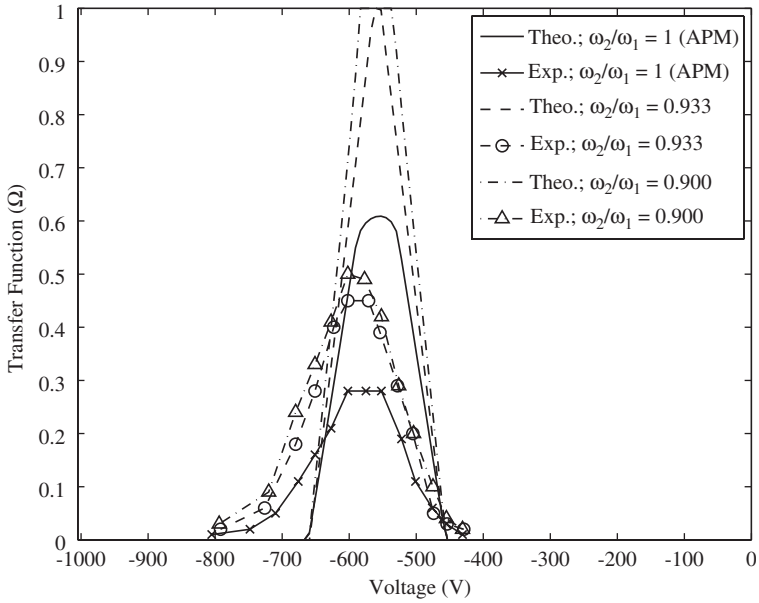

Fig. 5. Transfer function of the Couette CPMA classifying 220 nm PSL particles at various values of $\hat{\omega}$ with $\omega_c = 6000$ rpm, $Q_{CPMA} = 0.3$ lpm.

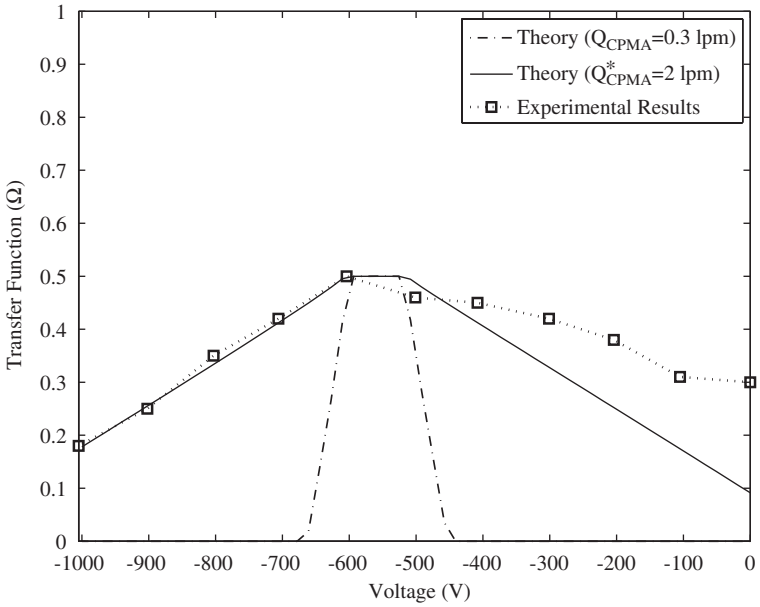

Fig. 6. Comparison of theoretical and experimental transfer functions of the Couette CPMA classifying 220 nm PSL particles at $\hat{\omega} = 0.867$ (beyond the Taylor limit) with $\omega_c = 6000$ rpm, $Q_{CPMA} = 0.3$ lpm.

Fig. 6 shows an example when the Couette CPMA is operated in a region where Taylor vortices are present (i.e. $\hat{\omega} < 0.890$). The figure shows the experimental transfer function and two theoretical transfer functions. The theoretical transfer functions shown are the expected transfer functions *without* Taylor vortices at two different flow rates; $Q_{CPMA} =$ 0.3 and 2 lpm (for comparison purposes the theoretical transfer functions have been scaled to account for inertial effects). During the experiment the actual flow rate through the Couette CPMA was 0.3 lpm. The figure shows that the experimental transfer function is very broad; much broader than the theoretical transfer function at 0.3 lpm. The

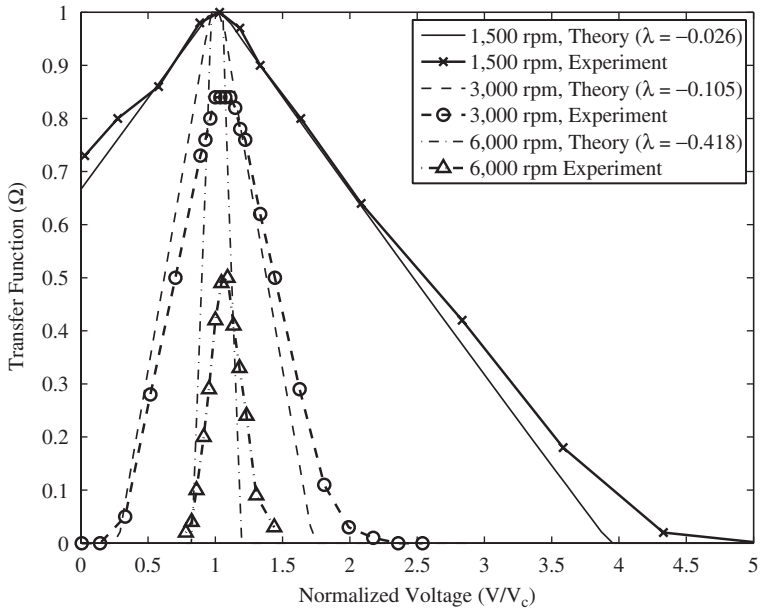

Fig. 7. Transfer function of the Couette CPMA classifying 220 nm PSL particles at various values of λ with $Q_{\mathrm{CPMA}} = 0.3$ lpm and rotational speeds of 1500, 3000, and 6000 rpm.

broadness of the transfer function is due to the fact that the residence time of the particles is greatly reduced when Taylor vortices are present. It has been shown that Taylor vortex flow with an axial flow has a 'winding' or 'bypass' flow that winds through the vortices (Ohmura, Suemasu, & Asamura, 2005). The 'winding' flow is 'a strong stream of fluid winding around vortices that do not fill the annular gap and appear alternately displaced toward the inner and outer cylinders' (Wereley & Lueptow, 1999). The particles travel through the classifier on this strong stream and the particle residence time is greatly reduced and the transfer function becomes much broader. Theoretically we can model this reduced transfer time by increasing the flow rate in the model. Fig. 6 shows the transfer function of the classifier with an apparent flow rate (Q^*_{CPMA}) of 2 lpm. The theoretical transfer function with $Q^*_{\mathrm{CPMA}} = 2$ lpm fits the experimental data much better, except on the right-hand side of the figure where the surfactant or multiply charged particles have also been classified. This result seems to suggest that the winding flow does reduce the residence time of particles in the Couette CPMA, which increases the width of the transfer function. Therefore, the Couette CPMA should not be operated in the Taylor vortex regime.

4.3. Examples concerning differences in λ

The dimensionless constant λ (see Eq. (2)) determines the shape of the transfer function. For the Couette CPMA the theoretical amplitude of the transfer function is always one. However, the width of the transfer function decreases as $|\lambda|$ increases. Fig. 7 shows the transfer function of the Couette CPMA at different values of λ. The 220 nm PSL particles were classified at three different rotational speeds; 1500, 3000, and 6000 rpm. The values of λ corresponding to these speeds were: -0.026, -0.105, and -0.418, respectively. The voltage axis was normalized for comparison purposes. The figure shows that as $|\lambda|$ increases the transfer function becomes narrower as theory predicts. The figure also shows that as the rotational speed increases (larger $|\lambda|$) the particle losses due to inertial effects also increase.

4.4. Calibrated density measurements with the DMA–CPMA system

A DMA and Couette CPMA can be used together to measure many important particle properties such as particle density, fractal dimension, aerosol mass distributions, and dynamic shape factors. The Couette CPMA can be used to determine the mass of particles and that mass data can be used together with other data, such as size, to determine

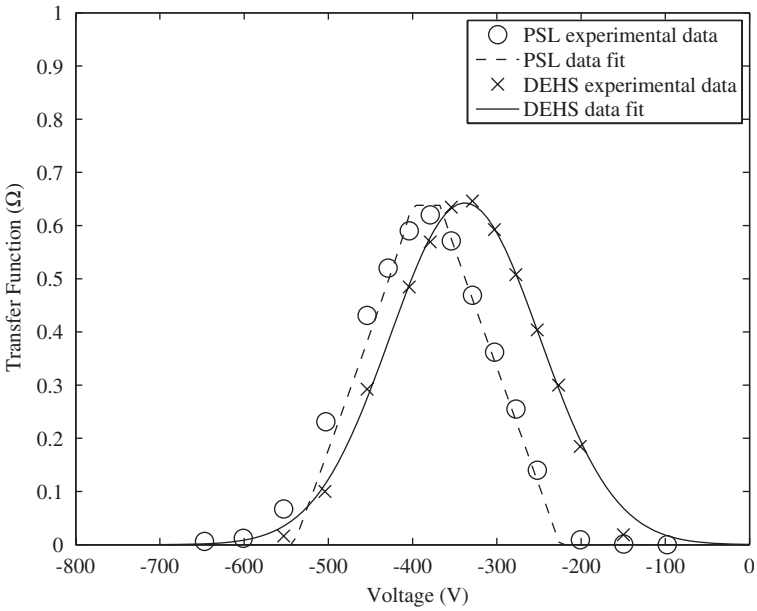

Fig. 8. Transfer function of the Couette CPMA classifying 299 nm PSL and DEHS particles with $\omega_c = 3000$ rpm and $\hat{\omega} = 0.90$.

other particle properties. Previously, it has been shown that an APM and DMA can be used together to determine the following properties: the density of spherical particles and effective density of non-spherical particles (Ehara & Shin, 1998; McMurry, Wang, Park, & Ehara, 2002; Park, Cao, Kittelson, & McMurry, 2003), fractal dimension (Park, Cao, et al., 2003; Park, Kittelson, & McMurry, 2004), aerosol mass distributions and mass concentrations (Park, Kittelson, & McMurry, 2003), and dynamic shape factors (McMurry et al., 2002; Park, Kittelson, & McMurry, 2004). It should also be noted that Park, Kittelson, and McMurry (2004) and Park, Kittelson, Zachariah, and McMurry (2004) measured the material density of agglomerate particles by using a DMA, an APM, and a transmission electron microscope (TEM).

To demonstrate the relative accuracy of the DMA–CPMA system, the density of DEHS particles was measured. In this work the DMA–CPMA system was calibrated with PSL particles to eliminate the systematic errors mentioned above, so that the uncertainty in the measurements could be minimized.

McMurry et al. (2002) showed that the density of particles can be accurately measured with the DMA–CPMA method by calibrating the system with PSL particles. This was done by setting the DMA voltage for the maximum penetration of PSL particles and then stepping the voltage of the CPMA to find the voltage where the maximum transfer function occurred ($V_{c,PSL}$). Then the unknown 'test' particle can be classified with the DMA at the same settings and again the voltage of the CPMA can be stepped to find the voltage of maximum penetration ($V_{c,test}$). Using this method the true density of spherical particles (ρ_p) can be found from Eq. (5) where

$$\frac{m_{test}}{m_{PSL}} = \frac{neV_{c,test}/\omega_c^2 r_c^2 \ln(r_2/r_1)}{neV_{c,PSL}/\omega_c^2 r_c^2 \ln(r_2/r_1)}, \tag{8}$$

$$\frac{\rho_{p,test}\pi d_{ve}^3/6}{\rho_{PSL}\pi d_{PSL}^3/6} = \frac{V_{c,test}}{V_{c,PSL}}, \tag{9}$$

$$\rho_{p,test} = \rho_{PSL}\frac{V_{c,test}}{V_{c,PSL}}, \tag{10}$$

using the fact that for a spherical particle $d_{ve} = d_{PSL}$, where d_{ve} is the volume equivalent diameter and ρ_{PSL} is the density of PSL (1050 kg/m^3).

Fig. 8 shows the transfer function of the Couette CPMA classifying mobility-selected PSL and DEHS particles with a diameter of 299 nm. Since the DEHS particles are spherical the material density of the particles can be found with

Table 2
Summary of DEHS density measurements

Particle size (nm)	Test number	Measured	
		Density (g/cm^3)	% error (%)
299	1	0.939	+2.7
	2	0.938	+2.6
	3	0.926	+1.3
152	1	0.885	−3.2
	2	0.917	+0.3
	3	0.933	+2.0

Eq. (10). The PSL data were fitted to the non-diffusion model and the DEHS data were fitted to a normal probability density function as described in Section 3. From the data fits $V_{c,PSL}$ and $V_{c,test}$ were found, and the density of the particles were found to be 0.926 g/cm^3. The actual density of DEHS is 0.914 g/cm^3, therefore the measurement was 1.3% higher than expected. Table 2 summarizes experimental results of particle density measurements of 152 and 299 nm DEHS particles measured with the Couette CPMA and DMA. The results show the density of particles can be measured to within approximately 3%, which is similar to the uncertainty in density measurements made with the APM (5%) reported by McMurry et al. (2002).

5. Conclusions and summary

The Couette CPMA classifies particles by their mass-to-charge ratio. A prototype Couette CPMA was built, tested, and compared with the theoretical models developed earlier (Olfert & Collings, 2005). The prototype Couette CPMA was tested over a range of particle sizes, speed ratios ($\hat{\omega}$), and λ's. It was found that the transfer function of the Couette CPMA agreed well with the theoretical model, except for a slight, systematic offset and particle losses due to inertial effects. This offset can be compensated for by calibrating the instrument with a calibration particle such as PSL. By comparing $\hat{\omega}$ it was found that the Couette CPMA does have a better transfer function than the APM and that exceeding the Taylor limit for fluid stability results in a much broader transfer function due to the winding flow established by the Taylor vortices. It was also found that impaction losses in the Couette CPMA can be significant at certain operational conditions and an improved method of moving particles into and out of the classification region would improve the performance of the classifier. It was also shown that by increasing $|\lambda|$, the transfer function narrows as theory predicts. Experimental results also show that a DMA–CPMA system can be used to measure particle density. The density of the DEHS particles measured with the prototype Couette CPMA was typically within 3% of the actual density of the liquid.

References

Dalley, J. E. J., Greenaway, R. S., Ulanowski, Z., Hesse, E., & Kaye, P. H. (2005). Measurement of the charge of airborne 3–10 μm spherical dielectric particles charged in an AC unipolar charger. *Journal of Aerosol Science*, *36*, 1194–1209.

Ehara, K. (1995). *Aerosol mass spectrometer and method of classifying aerosol particles according to specific mass*. US patent 4,428,220.

Ehara, K., Hagwood, C., & Coakley, K. J. (1996). Novel method to classify aerosol particles according to their mass-to-charge ratio—Aerosol particle mass analyzer. *Journal of Aerosol Science*, *27*, 217–234.

Ehara, K., & Shin, S. (1998). Measurement of density distribution of aerosol particles by successive classification of particles according to their mass and diameter. *Journal of Aerosol Science*, *29*(Suppl. 1), S19–S20.

Fukushima, N., Tajima, N., Ehara, K., & Coakley, K. J. (2005). Performance characteristics of the aerosol particle mass analyzer. In *American association for aerosol research 2005 annual conference*, Poster.

Kasper, K., & Berner, A. (1980). Diameters of airborne latex spheres measured with a cylindrical aerosol centrifuge. *Journal of Colloid and Interface Science*, *80*, 459–465.

Knollenberg, R. G. (1989). The measurement of latex particle sizes using scattering ratios in the Rayleigh scattering size range. *Journal of Aerosol Science*, *20*, 331–345.

McMurry, P. H., Wang, X., Park, K., & Ehara, K. (2002). The relationship between mass and mobility for atmospheric particles: A new technique for measuring particle density. *Aerosol Science and Technology*, *36*, 227–238.

Megaw, W. J., & Wells, A. C. (1972). The size of airborne Dow polystyrene spheres. *Journal of Aerosol Science*, *3*, 1–6.

Ohmura, N., Suemasu, T., & Asamura, Y. (2005). Particle classification in Taylor vortex flow with an axial flow. *Journal of Physics: Conference Series*, *14*, 64–71.

Olfert, J. S. (2005). A numerical calculation of the transfer function of the fluted centrifugal particle mass analyzer. *Aerosol Science and Technology*, *39*, 1002–1009.

Olfert, J. S., & Collings, N. (2005). New method for particle mass classification—The Couette centrifugal particle mass analyzer. *Journal of Aerosol Science*, *36*, 1338–1352.

Park, K., Cao, F., Kittelson, D. B., & McMurry, P. H. (2003). Relationship between particle mass and mobility for diesel exhaust particles. *Environmental Science and Technology*, *37*, 577–583.

Park, K., Kittelson, D. B., & McMurry, P. H. (2003). A closure study of aerosol mass concentration measurements: Comparison of values obtained with filters and by direct measurements of mass distributions. *Atmospheric Environment*, *37*, 1223–1230.

Park, K., Kittelson, D. B., & McMurry, P. H. (2004). Structural properties of diesel exhaust particles measured by transmission electron microscopy (TEM): Relationships to particle mass and mobility. *Aerosol Science and Technology*, *38*, 881–889.

Park, K., Kittelson, D. B., Zachariah, M. R., & McMurry, P. H. (2004). Measurement of inherent material density of nanoparticle agglomerates. *Journal of Nanoparticle Research*, *6*, 267–272.

Reavell, K., & Rushton, M. (2004). UK patent application number 0417657.4.

Taylor, G. I. (1923). Stability of a viscous liquid contained between two rotating cylinders. *Philosophical Transactions of the Royal Society of London*, *223*, 289–343.

Wereley, S. T., & Lueptow, R. M. (1999). Velocity field for Taylor–Couette flow with an axial flow. *Physics of Fluids*, *11*, 3637–3649.

White, F. M. (1994). *Fluid mechanics*. New York: McGraw-Hill.

Zelenyuk, A., Cai, Y., Chieffo, L., & Imre, D. (2005). High precision density measurements of single particles: The density of metastable phases. *Aerosol Science and Technology*, *39*, 972–986.